Induction of PARP7 Creates a Vulnerability for Growth Inhibition by RBN2397 in Prostate Cancer Cells

Chunsong Yang[1], Krzysztof Wierbiłowicz[1,2], Nicki Abianeh[3], Tarek Abbas[3], Aakrosh Ratan[2], David Wotton[1], Bryce M Paschal[1]
[1]Department of Biochemistry and Molecular Genetics,
[2]Center for Public Health Genomics,
[3]Department of Radiation Oncology,
University of Virginia School of Medicine, Charlottesville, VA 22908, USA

Correspondence.
Bryce M Paschal, PhD, University of Virginia, Multistory Building 7021 Research Lab, 1335 LEE ST, Charlottesville, VA 22908, paschal@virginia.edu,Tel 434.243.6521

Running Title. Parp7 in prostate cancer

Keywords. Androgen, AR, AHR, ADP-ribosylation, PARP

ABSTRACT

The ADP-ribosyltransferase PARP7 modulates protein function by conjugating ADP-ribose to the side chains of acceptor amino acids. PARP7 has been shown to affect gene expression in prostate cancer cells and certain other cell types by mechanisms that include transcription factor ADP-ribosylation. Here, we use a recently developed catalytic inhibitor to PARP7, RBN2397, to study the effects of PARP7 inhibition in androgen receptor-positive and androgen receptor-negative prostate cancer cells. We find that RBN2397 has nanomolar potency for inhibiting androgen-induced ADP-ribosylation of the androgen receptor. RBN2397 inhibits the growth of prostate cancer cells in culture, mainly when cells are treated with ligands that either activate the androgen receptor, or the aryl hydrocarbon receptor, and induce PARP7 expression. We show that the growth inhibitory effects of RBN2397 are distinct from its enhancement of interferon signaling recently shown to promote tumor immunogenicity. RBN2397 treatment also induces biochemical trapping of PARP7 within the nucleus, which is reminiscent of how inhibitors such as Olaparib affect PARP1. Because RBN2397 can affect cancer cells through multiple mechanisms, PARP7 may be an actionable target in prostate cancer.

INTRODUCTION

The PARP family of enzymes contributes to a variety of cellular pathways, many of which occur in the nucleus and involve events associated with the regulation of chromatin structure, transcription, and DNA damage signaling and DNA repair[1, 2]. PARP enzymes contain a conserved catalytic domain that uses NAD^+ as a co-factor for ADP-ribose conjugation to the side chains of acceptor amino acids, and in the case of enzymes that generate polymers, conjugation to ADP-ribose itself[3]. The founding member of the PARP family, poly-ADP-ribosyltransferase 1 (PARP1) has been a major focus in the field since its discovery. Detailed, mechanistic analysis of PARP1 has been complemented by the development of highly specific compounds that compete for NAD^+ binding, and as a consequence, inhibit PARP1 enzymatic function[4]. Clinical trials with PARP1 inhibitors such as Olaparib have shown patient benefit in ovarian, breast, and prostate cancer,

particularly in tumors that harbor mutations in DNA repair genes, notably *BRCA1/2* and *ATM*[5].

Most PARP family members mediate a single round of ADP-ribose attachment and are categorized functionally as mono-ADP-ribosyltransferases[3]. Mono-ADP-ribosylation provides a post-translational mechanism for modulating protein function, likely in a reversible manner since cells encode hydrolases that can remove ADP-ribose from amino acids[6]. TIPARP/PARP7, a mono-ADP-ribosyltransferase expressed in multiple cell and tissue types, was characterized as a key effector of signaling and gene expression mediated by the aryl hydrocarbon receptor (AHR) in the context of detoxification pathways in liver[7]. Our group identified PARP7 in a prostate cancer cell signaling pathway that controls assembly of a multi-subunit complex containing the androgen receptor (AR) [8]. In this nuclear pathway, PARP7 “writes” ADP-ribose onto cysteine (Cys) residues in AR. The ADP-ribosyl-Cys sites are subsequently “read” by macrodomains in PARP9; this provides a highly selective mechanism for assembling a complex that contains AR, PARP9, and the ubiquitin E3 ligase DTX3L. Depletion of the DTX3L affects the expression of a subset of AR-regulated genes[8], suggesting PARP7 and assembly of the complex has a regulatory role in transcription. PARP7 has been functionally linked to other transcription factors including the estrogen receptor and liver X receptors [9, 10]. It seems plausible that PARP7 contributes to a wide variety of gene expression pathways through mechanisms that include, but are not limited to, transcription factor ADP-ribosylation.

PARP7 also exerts an effect on transcription through a signaling-based mechanism involving the kinase, TBK1. PARP7 negatively regulates TBK1 kinase activity, which restrains phosphorylation and activation of the transcription factor IRF3[11]. In this pathway, PARP7 was proposed to serve as a brake for sensing cytosolic nucleic acids that trigger Type I IFN signaling [12]. Ribon Therapeutics developed RBN2397, a first-in-class mono-ADP-ribosyltransferase inhibitor, and showed it blocks PARP7 negative regulation of TBK1[12]. Treating cells with RBN2397 promotes TBK1 phosphorylation of IRF3, restoration of Type I IFN signaling and effects on gene expression, and enhances tumor immunogenicity in lung cancer models[12]. These data provide the rationale for targeting PARP7 with RBN2397, which is orally bioavailable and under evaluation in a Phase 1 clinical trial (NCT04053673).

Here, we explore the use of RBN2397 as a PARP7 inhibitor in prostate cancer cell lines. Consistent with a previous report[12], RBN2397 has selectivity for PARP7 versus other PARP family members in ADP-ribosylation when assayed using core histones as substrates. In cells, we show that RBN2397 has nanomolar potency for inhibiting PARP7 ADP-ribosylation of AR. We determined that RBN2397 inhibits the growth of prostate cancer cells dependent on transcriptional induction of PARP7, that can be achieved by treating cells with androgen to activate AR, or with ligands that activate AHR. RBN2397 exerts a nuclear trapping effect on PARP7, analogous to the effects of clinically-used inhibitors to PARP1[13, 14]. Finally, we used chemical inhibitors to TBK1 and JAK1/2 to show that RBN2397 inhibition of prostate cancer cell growth can be distinguished from the RBN2397 effect on

PARP7 regulation of Type I IFN signaling. The available data indicate that PARP7 inhibition with RBN2397 exerts effects on cancer cells through multiple mechanisms.

RESULTS

RBN2397 reduces the growth of lung cancer models by inhibiting PARP7, restoring IFN signaling, and increasing tumor immunogenicity[12]. We evaluated whether RBN2397 has potential utility in prostate cancer using biochemical approaches and cell growth assays in AR-positive (AR+) and AR-negative (AR-) prostate cancer lines. In previous work we reported that PARP7 directly ADP-ribosylates eleven Cys residues in AR[8]. AR ADP-ribosylation is induced by androgen in prostate cancer cells because the *PARP7* gene is a direct target of AR, and because PARP7 selectively ADP-ribosylates the agonist conformation of AR [8, 15]. Androgen-induced ADP-ribosylation of AR in cells and detection with fluorescently labeled Af1521 (Fl-Af1521) on blots [16] provides a sensitive assay to assess the effect of chemical inhibition of PARP7 in cells. To this end, we treated PC3-AR cells with synthetic androgen (R1881) to induce *PARP7* transcription and AR-ADP-ribosylation, in the absence and presence of the PARP7 inhibitor RBN2397. We found that AR ADP-ribosylation was reduced by 1 nM RBN2397 and essentially eliminated by 3 nM RBN2397 (**Fig. 1A**). RBN2397 also inhibited androgen-induced ADP-ribosylation of AR in VCaP cells (**Fig. 1B**). The selectivity of RBN2397 for PARP7 versus the PARP family was characterized previously[12], primarily with biophysical assays that measure competitive binding with NAD^+, which is the basis of how RBN2397 inhibits PARP7 enzyme function[12]. We measured the effect of RBN2397 on substrate ADP-ribosylation using recombinant PARP7 and PARP1 and a mixture of Histone H2A and H2B to determine EC_{50} values. In vitro, the EC_{50} of RBN2397 for PARP7 is approximately 7.6 nM, whereas the EC_{50} of RBN2397 for PARP1 is 110 nM (**Fig. 1C**). In the presence of 7.6 nM RBN2397, there is relatively little inhibition of other PARP enzymes, including family members with expression levels in prostate tumors that exceed the level of PARP7 (**Fig. 1D**).

RBN2397 treatment of PC3-AR cells also increases the level of PARP7 protein detected by immunoblotting, suggesting the inhibitor might stabilize PARP7 protein (**Fig. 1A**). We performed a time course of cycloheximide treatment and found RBN2397 increases the protein half-life of PARP7 approximately 4-fold (**Fig. 1E**). Stabilization of PARP7 protein provides additional evidence for the on-target effects of RBN2397 in prostate cancer cells. Lastly, we examined the effect of RBN2397 on PARP7 auto-ADP-ribosylation, as auto-modification is a common biochemical property of PARP enzymes. RBN2397 treatment of cells eliminated PARP7 auto-ADP-ribosylation in cells, detected by immunoprecipitation of PARP7 and using Fl-Af1521 to probe for mono-ADP-ribose (**Fig. 1F**). Treating cells with the proteasome inhibitor MG132 blocks PARP7 degradation and increases the level of auto-ADP-ribosylated protein (**Fig. 1F**).

We examined the effects of RBN2397 on growth with cell lines used to model prostate cancer and therapy resistance. VCaP cells encode WT AR and the V7 variant, and are used to model castrate-resistance owing to amplification of *AR*. CWR22Rv1 is an informative model for therapy resistance mediated by *AR* splice

variants that lack the ligand binding domain. PC3-AR is a PC3 derivative engineered to express WT AR, which drives a gene expression profile that overlaps other prostate lines[17]. PC3 cells are AR negative, resistant to therapies based on androgen deprivation, highly motile, and used to study prostate cancer metastasis. Overall, treating the four prostate lines with RBN2397 had little or no effect on growth. RBN2397 slightly increased the growth of VCaP, it reduced the growth of CWR22Rv1 and PC3 cells, and had no significant effect on PC3-AR cells (**Fig. 2A**). While the effects of RBN2397 treatment were statistically significant in some cases, the effects were quantitatively small. Reasoning that low PARP7 expression levels might limit the effect of RBN2397 on cell growth, we treated cells with androgen (R1881) to activate AR and induce PARP7 expression. We found that RBN2397 was growth inhibitory in androgen-treated VCaP, CWR22Rv1, and PC3-AR cells (**Fig. 2A**). It is well established that androgen treatment is growth-repressive in some prostate cancer lines. R1881 was growth inhibitory in VCaP and PC3-AR cells; RBN2397 further reduced the growth of VCaP and PC3-AR cells, and in CWR22Rv1 cells had greater effects on growth in the presence of R1881 (**Fig. 2A**). Dose response curves for cell growth in the presence of androgen revealed RBN2397 had half-maximal effects in the low nanomolar range (**Fig. 2B; Supplementary Table 1**), which is consistent with its potency for inhibiting PARP7 ADP-ribosylation of AR in cells (**Fig. 1A**). Growth inhibition by RBN2397 does not involve accumulation of cells in a specific phase of the cell cycle, though within the data a G1 effect of androgen is apparent in VCaP and PC3-AR cells (**Supplemental Fig. 1A**). By phase contrast microscopy, RBN2397 promotes the appearance of rounded cells (**Fig. 2C**) and RBN2397 can increase the number of dead cells detected by Trypan blue staining in CWR22Rv1 and PC3-AR cells (**Fig. 2D**). Overall, the data suggest that the growth inhibition by RBN2397 occurs through several mechanisms, but the effects do not seem to involve blocking the cell cycle at a specific phase to the extent it can be measured by DNA content.

We next tested if the androgen-dependence of the RBN2397 growth inhibition is associated with PARP7 expression. Using an siRNA that targets *PARP7* (*siPARP7*), we determined the cell growth reduction caused by RBN2397 in androgen-treated PC3-AR cells was reduced by *PARP7* knockdown (**Fig. 3A**). PARP7 protein levels revealed by immunoblotting after R1881 treatment are very low, but the additional treatment with RBN2397 stabilizes PARP7 protein and facilitates its detection by immunoblotting (**Fig. 3A-C**). Reducing PARP7 levels with *shPARP7* (stably-expressed) gave similar results. Though the efficiency of PARP7 depletion, and the growth differences ±RBN2397 in control and *shPARP7* cell lines were quantitively small, the effect of PARP7 knockdown was statistically significant in both PC3-AR and CWR22Rv1 cells (**Fig. 3B, C**).

One mechanism by which androgens repress the growth of prostate cancer lines through AR is by induction of the CYCLIN-dependent kinase inhibitor p21 [18]. Given the growth repressive effects of RBN2397 were associated with androgen treatment, we tested whether the RBN2397 effect on growth involves p21 expression. By immunoblotting, p21 protein expression in VCaP and PC3-AR cells is positively regulated by androgen, and p21 levels were increased further by RBN2397

treatment (**Fig. 3D**). The levels of p21 were not affected by androgen in AR-positive CWR22Rv1 cells, and as expected, there was no androgen effect in AR-negative PC3 cells (**Fig. 3D**). Using siRNA to reduce p21 expression, we found that p21 depletion resulted in a partial rescue of the growth inhibitory effect of RBN2397 (**Fig. 3E**). Similarly, eliminating p21 expression by making a deletion in the *CDKN1A* gene in PC3-AR cells (CRISPR-CAS9) partially rescued the effects of RBN2397 (**Fig. 3F**). These data show that in the context of androgen signaling, the growth inhibitory effects of RBN2397 can be partly mediated through p21, but this mechanism is not operational in all prostate cancer cell lines.

Growth inhibition by RBN2397 in androgen-treated VCaP, CWR22Rv1, and PC3-AR cells raises the intriguing possibility that PARP7 might be an actionable target in prostate cancer. As an alternative approach for inducing *PARP7* in prostate cancer cells, we turned to the transcription factor AHR, a member of the basic helix-loop-helix /Per-AHR nuclear translocator-Sim protein family. AHR is known to control PARP7 expression in other settings, and has been studied in the context of detoxification mechanisms in liver[7, 19].

We tested two ligands with potent AHR agonist activity for PARP7 induction in prostate cancer. 6-Formylindolo[3,2-b]carbazole (FICZ) is a naturally occurring tryptophan photoproduct, and 10-Chloro-7*H*-benzimidazo[2,1-*a*]benz[d*e*]isoquinolin-7-one (10-CL-BBQ, or BBQ in short) is a synthetic ligand. FICZ and BBQ induce AHR target genes through a chaperone-mediated mechanism[20]. FICZ and BBQ (10-100 nM) were both effective for sensitizing cells to growth inhibition by RBN2397 (**Supplementary Table 1**), and the growth inhibitory effect was associated with PARP7 protein stabilization detected by immunoblotting (**Fig. 4A**). These data show that PARP7 can be induced by AHR in AR-positive (CWR22Rv1 and VCaP) and AR-negative (PC3 and DU145) prostate cancer cells for the purpose of sensitizing cells to RBN2397. Combining PARP7 induction with BBQ and RBN2397 treatment reduced the protein levels of CYCLIN A and CYCLIN B in PC3, DU145, and CWR22Rv1, though the effect was small and not observed in VCaP cells (**Fig. 4B**). BBQ and RBN2397 treatment increased the G1 fraction in PC3 and DU145 cells, and slightly reduced the S-phase fraction in CWR22Rv1 cells (**Supplementary Fig. 1B**). By phase contrast microscopy there was a reduction in the number of adherent cells in PC3, DU145, and CWR22Rv1 cells treated with BBQ and RBN2397 (**Fig. 4C**), which is consistent with our finding that combining BBQ and RBN2397 increased the number of Trypan blue-positive cells in PC3, DU145, and CWR22Rv1 cells (**Fig. 4D, E**).

The cell growth and immunoblotting data for PARP7, CYCLIN A, CYCLIN B, and the Trypan blue detection of dead cells, imply the BBQ and RBN2397 combination is more effective in PC3, DU145, and CWR22Rv1 than in VCaP cells (**Supplementary Table 1**). The RBN2397 dose response curves for cell growth were also consistent with this notion, where PC3 and DU145 cells were inhibited by nanomolar concentrations of RBN2397 and the overall response was greater than VCaP cells (**Fig. 4F-H**). To determine if the RBN2397 effect is dependent on PARP7 expression, we compared the RBN2397 sensitivity of control and *PARP7* knockdown cells treated with BBQ. Although the *PARP7* knockdown was

partial, the RBN2397 effect was reduced significantly in *shPARP7* compared with *shGFP* cells (**Fig. 4I, J**). Taken together, the data show that RBN2397 can be used to inhibit growth in prostate cancer cells where PARP7 is induced by AHR signaling.

The cellular effects of RBN2397 in preclinical models of lung cancer were attributed to reversal of a PARP7-TBK1 inhibitory mechanism, resulting in IRF3 phosphorylation, restored IFN signaling, and increased tumor immunogenicity [12]. Because IRF3 can also regulate the cell cycle [21], we queried whether TBK1 activity and IFN signaling are involved in the growth inhibitory effects of RBN2397 in prostate cancer cells. To this end, we employed specific inhibitors to TBK1 (GSK8612; GSK) and JAK1/2 (Ruxolitnib; Ruxo) in prostate cancer cell lines and induced PARP7 via AHR (PC3, DU145) and AR (PC3-AR)(**Fig. 5**). In PC3 cells, RBN2397 treatment increased the basal level of phospho-STAT1, an effect that was eliminated by JAK1/2 (Ruxo) and TBK1 (GSK) inhibitors (**Fig. 5A**). These data are consistent with TBK1 acting upstream of JAK1/2 in PC3 prostate cancer cells, as shown in other cell types [12]. Induction of PARP7 by the AHR ligand BBQ does not further increase STAT1 phosphorylation, suggesting the relatively low, basal level of PARP7 expression is sufficient for the RBN2397 effect on STAT1 phosphorylation in PC3 cells (**Fig. 5A**, left panel). This contrasts with the growth inhibitory effect of RBN2397, which is responsive to PARP7 expression induced by treating cells with ligands to AHR and AR (**Figs. 2, 4**).

The growth inhibitory effect of RBN2397 in PC3 cells is not reversed by JAK1/2 and TBK1 kinase inhibition with Ruxo and GSK, respectively (**Fig. 5A**, right panel). This result indicates the RBN2397 enhancement of IFN signaling implied by STAT1 phosphorylation (**Fig. 5A**, left panel) does not drive growth inhibition in PC3 cells. Consistent with this view, induction of IFN signaling only slightly reduces PC3 cell growth (**Fig. 5A**, right panel). In DU145 cells, RBN2397 has no obvious effect on basal STAT1 phosphorylation, despite the fact this line can activate JAK1/2-STAT signaling in response to IFNα (**Fig. 5B**, left panel). Thus, the growth reduction in DU145 cells caused by RBN2397 is not associated with an effect on STAT1 phosphorylation, and blocking JAK1/2 and TBK1 kinase function in this line slightly increases the growth inhibitory effect of RBN2397 (**Fig. 5B**, right panel). In PC3-AR cells, the signaling and growth data are very similar to PC3 cells; RBN2397 increases STAT1 phosphorylation, and blockade of JAK1/2 and TBK1 inhibitors largely eliminates the RBN2397 effect on STAT1 phosphorylation without affecting the growth inhibitory effect of RBN2397 (**Fig. 5C**). In VCaP and CWR22Rv1 cells, RBN2397 also has no obvious effect on basal STAT1 phosphorylation (**Supplementary Fig. 2**). From these data, we conclude the growth inhibitory effect of RBN2397 in prostate cancer cells is separable from its effects on IFN signaling that are linked to the kinase activities of JAK1/2 and TBK1.

Chemical inhibitors to PARP1 exert effects on cells by blocking enzyme function, but also via cytotoxic effects attributed to stabilizing PARP-chromatin interactions in a process termed trapping[13]. Drug-induced trapping of PARP1 can be detected biochemically by immunoblotting the detergent-resistant nuclear fraction [13]. To test if RBN2397 induces PARP7 trapping, we induced its expression in PC3-AR cells with R1881 $\pm$RBN2397 and performed cell fractionation and

immunoblotting. Antibodies for TUBULIN and LAMIN A were used to confirm the release of soluble proteins and recovery of Triton X-100 resistant, nuclear fraction. As shown in previous figures, R1881 treatment induces PARP7 which is released into the soluble fraction and virtually absent from the insoluble fraction (**Fig. 6A**, lanes 3 and 7). By contrast, the combination of R1881 and RBN2397 results in a pool of PARP7 that partitions to the insoluble fraction (**Fig. 6A**, lanes 4 and 8). In PC3 cells, inducing PARP7 using BBQ to activate AHR also resulted in PARP7 trapping (**Fig. 6B**, lanes 4 and 8). The proportion of PARP7 trapped by RBN2397 treatment is similar to that observed when PARP1 is trapped by Olaparib and Niraparib [13]. RBN2397-mediated trapping of PARP7 on chromatin could contribute to the growth inhibition observed in prostate cancer cells.

It has been noted that for PARP1 and PARP7, genetic knockout is not equivalent to drug-induced inhibition of the enzymes[12, 13]. A logical interpretation of these findings is that drug binding to PARP1 and PARP7 exerts dominant negative effects that are in addition to the cellular changes associated specifically with preventing substrate ADP-ribosylation. We therefore considered the possibility that RBN2397 inhibition of prostate cancer cell growth involves a dominant negative effect. An alternative explanation, at least in prostate cancer cells, is that gene expression induced by AR and AHR creates a PARP7 dependency for cell growth. We chose the prostate cancer line C4-2b for this analysis. The basal level of PARP7 expression is extremely low in C4-2b cells, RBN2397 treatment alone has no effect on growth of these cells, and activation of AHR signaling sensitizes the cells to RBN2397 inhibition (**Fig. 6C**).

To test for a dominant negative effect of RBN2397-inhibited PARP7, ectopic PARP7 was expressed with an N-terminal Avi-tag in C4-2b cells (Avi-PARP7; **Fig. 6D**). Avi-PARP7 is enzymatically active in these cells since it ADP-ribosylates AR and the modification is blocked by RBN2397 (**Fig. 6D**). We found that expression of Avi-PARP7 is sufficient to confer a growth inhibition response to RBN2397 (**Fig. 6E**). Growth inhibition by RBN2397 in these cells is enhanced by AHR activation with BBQ, which increases the cellular level of PARP7 by induction of endogenous PARP7. The possibility that additional factors regulated through AHR contribute to the RBN2397 vulnerability cannot be excluded.

As a first step towards evaluating whether PARP7 levels in human prostate cancer are potentially actionable with RBN2397, we analyzed *PARP7* gene expression data from primary prostate tumors and metastatic *AR*+ and *AR*- prostate tumors[22]. To assess *PARP7* mRNA levels, we used data from the online resource recount3, which uniformly reprocesses publicly available RNA-seq datasets using a Monorail analysis pipeline [23]. This allowed us to compare transcriptomic data from different studies, including cell line and patient samples. We observe there are no changes in *PARP7* mRNA levels in primary tumors compared to normal prostate cells, but expression is reduced in metastatic tumors, and the difference is greater for metastatic tumors that are *AR*+ (**Fig. 7A**). Since growth inhibition by RBN2397 in cell culture is dependent on PARP7 expression, we used our RNA-seq data [17] from VCaP cells treated ±R1881 and processed through

recount3 to define basal and induced levels of *PARP7* (**Fig. 7A**). We then used the induced level to assign a cut-off for RBN2397 vulnerability in prostate tumors. By this criterion, 50% of primary tumors, 41% of metastatic *AR*- and 11% of *AR*+ tumors are predicted to have PARP7 expression levels that are sufficient for a response to RBN2397. Approximately 7% of metastatic prostate tumors (34/444) show genomic copy number alternations in *PARP7* **(Supplementary Fig. 3)**, which could contribute to protein expression levels.

To query how PARP7 expression is potentially regulated in tumors, we computed Spearman's rank correlation between *PARP7*, *AR*, and *AHR* gene expression. We found a moderate correlation between *PARP7-AR* expression ($r_s = 0.30$, $p < 0.001$, $n = 497$) and a strong positive correlation between *PARP7* and *AHR* expression ($r_s = 0.56$, $p < 0.001$, $n = 497$) (**Fig. 7B** left) in primary tumors. In both *AR*+ and *AR*- metastatic tumors the expression of *PARP7* and *AR* is not significantly correlated. However, the *PARP7-AHR* correlation is significant and is especially striking in *AR*- tumors ($r_s = 0.62$, $p < 0.001$, $n = 27$) (**Fig. 7B** middle, left). These results suggest that PARP7 expression in primary tumors could be influenced by AR and AHR, but in metastatic tumors the association with AR is lost, whereas the AHR influence is retained.

PARP7 has been proposed to restrain type I IFN signaling in lung cancer models, an effect relieved by RBN2397 [12]. We analyzed the PARP7 influence on type I IFN signaling in primary prostate tumors, using gene set variation analysis (GSVA) [24]. We found that lung cancer (LUAD) samples exhibit a much higher enrichment score and pathway activity for genes that are up-regulated in response to IFNα proteins (Type I IFN response) compared to prostate cancer (PRAD) samples (**Fig. 7C**). Moreover, the enrichment scores in LUAD shows an association with *PARP7* expression level, but this is not the case in PRAD (**Fig. 7C**). This suggests that either PARP7 does not influence Type I IFN signaling in primary prostate cancer, or that low levels of PARP7 are sufficient for the effect.

DISCUSSION

RBN2397 was developed by Ribon Therapeutics through optimization of an unselective mono-ADP-ribosyltransferase inhibitor [12]. Prior biochemical characterization of RBN2397 included using a probe displacement assay to demonstrate potent PARP7 inhibition (IC_{50} < 3 nM) and PARP7 selectivity (>50-fold) within the PARP family [12]. The same group assessed the effect of RBN2397 in PARP7-overexpressing cells by staining for MARylation [12, 25]. These and other data demonstrated the potency and selectivity of RBN2397 for PARP7. We characterized the effect of RBN2397 in prostate cancer cells, first by examining its ability to inhibit PARP7 ADP-ribosylation of AR. In prostate cancer cells, AR is a well-defined PARP7 substrate in which the ADP-ribosylation sites have been defined and characterized by mutagenesis[8]. In PC3-AR cells grown without androgen, virtually no ADP-ribose is detected on AR using Fl-Af1521 as a probe. Androgen treatment stimulates AR induction of endogenous PARP7, which then ADP-ribosylates AR on Cys sites primarily within its transactivation domain[8]. Biochemical and RNA-seq data are both consistent with PARP7 operating

as the androgen-regulated mono-ADP-ribosyltransferase that modifies nuclear AR in prostate cancer cells[8]. We found that low nanomolar concentrations of RBN2397 were sufficient to eliminate PARP7 ADP-ribosylation of AR in PC3-AR cells. RBN2397 treatment also prevented ADP-ribosylation of AR in VCaP cells, which demonstrates the effectiveness of RBN2397 in a setting where both PARP7 and its inducer/substrate (AR) are expressed from endogenous genes. Since RBN2397 can also inhibit PARP7 ADP-ribosylation of the estrogen receptor[9], RBN2397 might be useful to target signaling and growth in breast cancer.

A second finding in our study was that RBN2397 can inhibit the growth of prostate cancer cells, and that this occurs under conditions where PARP7 undergoes induced expression. In prostate cancer cell lines, PARP7 can be induced by treating cells with agonists for AR and AHR. The fact that there is little or no growth inhibition by RBN2397 prior to PARP7 induction suggests that the contribution of basal levels of PARP7 to cell growth of these cells in culture is minimal. Consistent with this view, DepMap analysis of VCaP and CWR22Rv1 cells show essentially no dependency on basal PARP7 expression. The growth inhibition by RBN2397 under conditions of PARP7 induction is suggestive of a dominant-negative effect of RBN2397-bound PARP7. Support for a dominant-negative mechanism derives from showing that ectopic PARP7 expression is sufficient to partially sensitize C4-2b cells to the growth inhibition by RBN2397. The growth inhibition of RBN2397 mediated through ectopic PARP7 was not as penetrant as the effect of RBN2397 in androgen-treated cells. The reduced penetrance might be due to an insufficient level of ectopic PARP7, or that androgen signaling through AR affects the expression of genes (in addition to *PARP7*) that promotes RBN2397 sensitivity. The basal level of PARP7 expression in some cell types such as NCI-H1373 is sufficiently high to confer a sensitivity to nanomolar RBN2397 [23]. In DepMap, NCI-H1373 cells display a *PARP7*-dependency.

The available data indicate that RBN2397 treatment of PARP7-expressing cancer cells has at least two effects, modulation of IFN signaling and reduction of cell growth. Whether these effects are linked or separate might be context-dependent, but our data favors the conclusion the effects are separate. RBN2397 enhancement of basal IFN signaling reported by Ribon was shown to occur because PARP7 can restrain TBK1 activity[11, 12]. We found that RBN2397 increases basal IFN signaling in PC3 and PC3-AR cells, as RBN2397 treatment was sufficient to increase phospho-STAT1 levels. The effect on phospho-STAT1 was abrogated by inhibiting either TBK1 or JAK1/2, suggesting the PARP7 effect on TBK1 and IFN signaling in PC3 cells is comparable to some other cell types[12]. And although IFN signaling can be growth repressive, the inhibitory effect of RBN2397 on cell growth in our experiments is not linked to the RBN2397 effect on IFN signaling. Thus, in the aforementioned experiment with TBK1 and JAK1/2 inhibitors that eliminated the RBN2397 enhancement of IFN signaling, blocking TBK1 and JAK1/2 did not alter the RBN2397 inhibition of cell growth. Moreover, RBN2397 had no obvious effect on basal IFN signaling in VCaP, CWR22Rv1, and DU145 cells, despite the fact RBN2397 inhibited growth of these cells. It was noted that RBN2397 can restore basal IFN signaling in CT26 cells without affecting cell proliferation in culture[12]. Whether PARP7 and RBN2397

affect IFN signaling, cell growth, or both, is expected to be dependent on PARP7 expression levels, and also the context. There is an association between the enrichment score for Type 1 IFN signaling in LUAD but not in PRAD. The contribution of PARP7 to IFN signaling might be dependent on the tumor type, but it is also possible that low levels of PARP7 are sufficient for an effect on TBK1.

Potential therapeutic benefits of RBN2397 could depend on PARP7 expression levels in tumors, particularly if the growth inhibitory mechanism in tumors involves a dominant negative effect as suggested by our cell culture data. Using recount3, we were able to compare RNA-seq data from cultured cell experiments to data from human prostate tumors. In VCaP cells, growth inhibition by RBN2397 required the addition of agonists for AR or AHR to induce PARP7 expression. Thus, PARP7 levels prior to, and after, androgen treatment of VCaP cells allowed us to define a threshold for PARP7 expression that results in a growth inhibitory response to RBN2397. Using this value as a cutoff, we estimate that about half of all prostate cancers should express sufficient PARP7 to be vulnerable to RBN2397. In *AR*-metastatic tumors, *PARP7* RNA levels are higher on average than *AR*+ tumors; this suggests *AR* status might help predict the utility of RBN2397 in a subgroup of patients.

In summary, we have shown that PARP7 expression confers sensitivity to growth inhibition by RBN2397. PARP7 expression levels can be regulated in prostate cancer cells using ligands for AR and AHR. PARP7 expression in primary prostate cancer tumors is correlated with both AHR and AR, which is logical given the *TIPARP* gene is a direct target of both transcription factors. Interestingly, the positive correlation between *AR* and *PARP7* expression appears to be lost in metastatic prostate tumors, suggesting that *PARP7* becomes highly dependent on AHR signaling for its expression in advanced disease. Combining AHR agonists with RBN2397 might provide PARP7-based strategy for inhibiting advanced prostate cancer.

MATERIALS AND METHODS

Drugs

Synthetic androgen methyltrienolone (R1881, Perkin-Elmer NLP005005MG), PARP7 inhibitor RBN2397 (RBN, Medchemexpress LLC HY-136174 or DCCHEMICALS DC31069), PARP1/2 inhibitor Veliparib (Selleck Chemical LLC S100410MG), 10-CL-BBQ (BBQ, Tocris Bioscience 63-215), FICZ (Medchemexpress LLC HY-12451), JAK1/2 inhibitor Ruxolitinib (Ruxo, Selleck Chemical LLC S13785MG), TBK1 inhibitor GSK8612 (GSK, Medchemexpress LLC HY-111941), IFNαA (MilliporeSigma IF007), proteasome inhibitor MG132 (Caymen Chemical 1001262810), Cycloheximide (MP Biomedicals 0219452701), (3-(4,5-dimethylthiazol-2-yl)-2,5-diphenyltetrazolium bromide (MTT, Tocris Bioscience 5224).

Antibodies

Rabbit antibodies to AR (1 µg/ml) and PARP7 (1 µg/ml) have been described[8, 26]. Commercial antibodies used were TUBULIN (1:10,000–20,000, mouse mAb TUB-1A2, Sigma T9028), HA tag (1:1,000,

mouse mAb 16b12, Covance A488-101L, also used for IP), p21 (1 µg/ml, mouse mAb SX118, BD Pharmingen 550827), AHR (1 µg/ml, Rabbit mAb JM34-10, Thermo Fisher Scientific MA5-32576), CYCLIN B1 (1:10,000, rabbit mAb Y106, Epitomics 1495-1), CYCLIN A (1:500, mouse mAb 6E6, Leica Microsystems NCL-CYCLIN A), STAT1α (1:1,000, rabbit mAb EPR4407, abcam ab109320), p-STAT1(Tyr701)(1:1,000, rabbit, Cell Signaling 9171), LAMIN A/C (1:40, mouse mAb JOL2, Millipore MAB3211), Alexa Fluor 680 donkey anti-Rabbit IgG(H + L) (1:20,000, Invitrogen A10043), IRDye800-conjugated anti-mouse IgG(H&L) (1:20,000, Rockland 610-132-121), and AR (mouse mAb G122-434, BD Pharmingen 554225, used for IP).

Cell culture

The growth mediums used are DMEM/F12 + 10% FBS for VCaP (ATCC CRL-2876), DMEM + 5% FBS for HEK293T (ATCC CRL-3216), RPMI1640 + 10% FBS for CWR22Rv1 (ATCC CRL-2505) and derivative cell lines, and RPMI1640 + 5% FBS for PC3 (ATCC CRL-1435), DU145 (ATCC HTB-81), PC3-AR and derivative cell lines; all the mediums were supplemented with 1% Pen/Strep. Cells were grown in the presence of 5% CO_2 and at 37 °C.

Lentivirus Production and Stable Cell Lines

PC3-AR, PC3-AR(*HA-PARP7*) and PC3-AR(*shGFP* or *shPARP7*) have been previously described[8].

Lentiviral plasmid *shPARP7* (or *shGFP* control, or pLH3/*AviTag-PARP7*) and two accessory plasmids pMD2g and psPAX2 (half as much as the lentiviral plasmid) were transfected into HEK293T cells with transfection reagent ViaFect (Promega PRE4981). After 16 hrs of transfection, growth medium was changed to DMEM + 35% FBS, and cells grew another 24 hrs. The growth medium which contained lentiviruses was transferred to a conical tube. Cell debris was removed with centrifugation at 1,000 RPM. The virus solution was passed through 0.4 μm filter, concentrated with Lenti-X Concentrator (Takara 631231). CWR22Rv1 or C4-2b cells were infected with virus for 24 hrs in the presence of 8 μg/ml of polybrene in the growth medium. After that, cells were changed into fresh growth medium, further grew for 2-3 doubling time, and then selected with 2 μg/ml of puromycin.

Generation of PC3-AR Cells with CDKN1A Deletion

A pair of sgRNAs targeting non-overlapping sequences within Exon 2 of the *CDKN1A* gene, encoding p21, were designed using Benchling, and cloned into the CAS9-expresssing pX330 expression vector (Addgene #42230). The following sgRNAs (sense strand) were used; sg-*p21*-1: 5'-GCGCCATGTCAGAACCGGCT-3', sg-*p21*-2: 5'-TTAGCGCATCACAGTCGCGG-3'. The sgRNA-containing pX330 plasmids were verified by Sanger sequencing (Eurofins) using U6-specific primers. To generate PC3-AR cells with *p21* deletion, the cells were grown to sub-confluency, and transiently transfected with the two CAS9-expressing plasmids (sg-*p21*-1 and sg-*p21*-2; 2.0 µg each), along with 0.5 µg pMSCVpuro vector (Clontech) containing a puromycin selectable marker. Transfections were performed using Lipofectamine 2000 (Invitrogen) according to the manufacturer's protocol. After 24 hours of transfection, cells were selected in the presence of puromycin (2 µg/ml) for 48 hours, after which single clones were isolated via serial dilutions of the transfected pool. To identify clones with

p21 deletion, we performed genotyping on DNA isolated from individual clones. Briefly, candidate clones were expanded in culture, lysed overnight at 55°C in lysis buffer (100 mM NaCl, 10 mM Tris-HCl pH 8, 25 mM EDTA, 0.5% SDS) supplemented with 20 µg of proteinase K. DNA was isolated from the lysed cells using phenol chloroform/isoamyl alcohol extraction. Genotyping was performed via PCR amplification of the targeted *p21* locus with primers flanking the two predicted CAS9 cleavage sites followed by Sanger sequencing (Eurofins). The following primers were used to amplify a 339 bp sequence spanning the two sgRNA target sites: p21-F: 5'-TCACCTGAGGTGACACAGCAAAGC-3', p21-R: 5'-GGCCCCGTGGGAAGGTAGAGCTT-3'. Immunoblotting of the individual p21 clonal knockout cells using an anti-p21 antibody was further used to confirm p21 deletion.

AR ADP-ribosylation

PC3-AR cells were grown in the growth medium supplemented with 2 nM R1881 +/- RBN2397 for 16-20 hours. After medium removal, cells were lysed in 1xSDS loading buffer (200mM Tris-HCl pH 6.8, 2% SDS, 10% glycerol and 3% β-Mercaptoethanol), and the lysates were heated at 95°C for 5 min, followed with sonication, centrifugation clearance, SDS-PAGE separation, and Nitrocellulose membrane transfer. The membrane was blocked in PBST+5% non-fat milk at room temperature for 45 minutes, followed with overnight 4°C incubation with 1 µg/ml Fl-Af1521 [16], room temperature PBST washing (5 minutes each for 5 times), and detection on ODYSSEY CLx (LI-COR).

Protein Half-Life Measurement

PC3-AR(*HA-PARP7*) cells, with or without 1 hour of 10 nM RBN2397 pre-treatment, were incubated with 0.1 mg/ml of Cycloheximide for indicated time periods. After medium aspiration, cells were lysed in 1xSDS-PAGE loading buffer, followed with heating, sonication, SDS-PAGE, HA-PARP7 Western Blot (with TUBULIN as control), and quantification on Odyssey CLx (LI-COR).

Cell Fractionation and Immunoprecipitation

All procedures were performed at 4°C. Cells were PBS washed once, scraped in Buffer A (20 mM Tris-HCl pH 7.5, 100 mM NaCl, 1 mM PMSF and 1 µM Veliparib), and collected with centrifugation (950×*g*, 5 min). Cells were lysed in Buffer B (20 mM Tris-HCl pH 7.5, 100 mM NaCl, 0.5% Triton X-100, 1 mM PMSF, 2 mM DTT, 2 mM EDTA, 1 µM Veliparib, and 5 µg/ml each of aprotinin/leupeptin/pepstatin) for 20 min. The Supernatants were collected after centrifugation (16,800×*g*, 20 min) and deemed as Tx-100 soluble fraction. The remaining pellets were washed once with Buffer B, resuspended in 1xSDS loading Buffer C (200mM Tris-HCl pH 6.8, 10% glycerol, 2% SDS and 3% β-Mercaptoethanol), sonicated, and then undergo centrifugation (16,800xg, 20 min) to get the supernatant which was deemed as Tx-100 residual fraction.

The Tx-100 soluble fraction was subjected to 4 µg antibody/2 µl packed Protein G magnetic beads per IP for binding for 3-4 hrs. The beads were separated under magnetic fields, followed with 5 times of washing with Buffer D (20 mM Tris-HCl pH 7.5, 100 mM NaCl, 0.1% Triton X-100, 1 mM DTT, 0.1 mM EDTA, 1 µM Veliparib, and 1 µg/ml each of Aprotinin/Leupeptin/Pepstatin), and then resuspended in 1xSDS loading Buffer C.

In Vitro PARP Assays

The assays were conducted by BPS Bioscience (San Diego, CA) in duplicates (PARP7) or triplicates (PARP1 etc) at Room Temperature for 2 hrs with reaction mixture containing PARP, inhibitors, β-NAD^+, and Biotin-β-NAD^+ in 96-well plates pre-coated with histone substrates. After enzymatic reactions, 50 µl of Streptavidin-horseradish peroxidase (prepared with Blocking Buffer) was added to each well and the plate was incubated at room temperature for an additional 30 min. The wells were washed again and 100 µl ELISA ECL substrate was added to each well. Luminescence was measured using a BioTek SynergyTM 2 microplate reader.

Cell Growth Assays

Cells (100 µl/well, most times 1:40 seeding in growth medium combined with drug R1881, RBN2397, BBQ, FICZ, Ruxo, GSK, IFNαA were grown at 37°C in 96-well plates in eight biological replicates, with medium changes every 2 days, till the no drug control cells reached relatively high cell density. The cells were washed once with PBS, incubated at 37°C for 2 hours with 100 µl of phenol-red free DMEM (for VCaP) or RPMI (for others) + 2% FBS + 0.25 mg/ml MTT, followed with medium removal, extraction with 100 µl of DMSO, and measurements on Synergy HT plate reader (BioTek). The numbers were subtracted of the background DMSO alone reading and quantified with Prism (GraphPad). Error bars represent standard deviation. P value **** <0.0001; *** <0.001; ** <0.01; * <0.05; ns, not significant.

siRNA Transfection

PC3-AR cells were transfected with 20 nM of Negative Control siRNA #1 (*siCon*, Ambion AM4635), *siPARP7* (sense strand 5'-AAUACUCUCAUCGAACGGAAGTT-3') or *si-p21* (sense strand 5′-AACAUACUGGCCUGGACUG-3') using Lipofectamine RNAiMAX (Invitrogen 56532). After 24 hrs of transfection, cells were re-plated into 96-well plates for cell growth assays. Percentages of cell growth inhibition at various RBN2397 concentration were compared between *siPARP7* (or *si-p21*) and *siCon*, with p value **** <0.0001; *** <0.001; ** <0.01; * <0.05. To confirm *PARP7* (or *p21*) knockdown, cells (24 hrs post-transfection) were re-plated into 6-well plates; 48 hrs later, cells were treated with R1881 and RBN2397 for another 24 hrs. Western blot was used to measure relative protein expression.

Cell Cycle Analyses

Cells were drug-treated for 48 hrs (slower growing VCaP and CWR22Rv1) or 24 hrs (faster growing PC3-AR and PC3), and then dispersed into single cells after trypsin treatments and pipetting. Cells were collected after centrifugation at 2,000 RPM at 4°C for 5 minutes. The cell pellets were PBS washed once, resuspended in 0.5 ml of cold PBS, mixed to 4.5 ml of cold 70% ethanol, and put on ice for over 2 hours. The cells were re-harvested by centrifugation and washed with PBS. Cells (~3.5 x 10^5) were resuspended in 0.1 ml of staining solution (PBS + 0.1% Triton X-100 + 80 µg/ml of Propidium Iodide + 0.2 mg/ml of RNase A), incubated at 37°C for 40 minutes, diluted with 0.4 ml of PBS + 0.1% Triton, measured on Attune NxT Cytometer (Thermo Fisher), and quantified with FCS Express 7 (De Novo Software).

Cell Morphology Analyses and Dead Cell Measurements

Cells were drug-treated for 6 days (slower growing VCaP and CWR22Rv1) or 3 days (faster growing PC3-AR and PC3). Pictures were taken under the EVOS Cell Imaging System (Thermo Fisher). Cells were also

dispersed into single cells after trypsin treatments and pipetting. Cells were collected after centrifugation at 2,000 RPM for 3 minutes. Cells were re-suspended in 1:1 of PBS and Trypan Blue Stain 0.4% (Invitrogen T10282), and counted on Countess II FL (Life Technologies).

RNA-seq data analysis. All of the data used in this study except GSVA analysis was obtained from recount3. Primary tumor data for prostate (PRAD) and lung (LUAD) used for GSVA analysis was generated by the TCGA Research Network: https://www.cancer.gov/tcga." TCGA PRAD RNA-seq dataset was prefiltered to keep only primary tumor and ffpe samples were removed (n=497). The metastatic castration-resistant prostate cancer (mCRPC) dataset from Fred Hutchinson Cancer Research Center (accn: SRP183532) [22] was prefiltered to keep only patient samples (n=98). Samples were divided into *AR*+ and *AR*- based on phenotypes evaluated in the original study[22]. For normal prostate analysis, we used the GTEx PROSTATE dataset (n=263). The Genotype-Tissue Expression (GTEx) Project was supported by the Common Fund of the Office of the Director of the National Institutes of Health, and by NCI, NHGRI, NHLBI, NIDA, NIMH, and NINDS. To assess the *PARP7* gene expression level cutoff we used our previously generated RNA-seq dataset[17], which also was obtained from recount3 to make it comparable with the rest of the data. For *PARP7* expression level comparison, we used counts per million (CPM) values calculated with the edgeR package in R. For correlation analysis we used Spearman correlation on log2 transformed TPM normalized data. For GSVA analysis [24]we used primary tumor samples from LUAD and PRAD TCGA cohorts. Samples were divided into high *PARP7* expressing (above upper quartile) and low *PARP7* expressing (below lower quartile). GSVA analysis was done using the GSVA Bioconductor R package for the MSigDB HALLMARK_INTERFERON_ALPHA_RESPONSE gene set.

ACKNOWLEDGMENTS
We thank Carlos S. Justo-Jaume for technical assistance, and Kendall Bromley for comments on the manuscript. The study was supported by NCI award R01CA214872 to B.M.P. and R01GM135376 to T.A.

FIGURE LEGENDS

Fig.1 NAD^+ competitive inhibitor RBN2397 blocks PARP7-mediated ADP-ribosylation of the androgen receptor (AR) in cells.
(A) Effect of RBN2397 concentration (12 pM to 81 nM) on androgen-induced ADP-ribosylation of AR in PC3-AR cells treated for 17 hrs prior to harvest.
(B) RBN2397 inhibits androgen-dependent AR ADP-ribosylation in VCaP prostate cancer cells. AR was immunoprecipitated and protein and ADP-ribose detected by immunoblotting (upper panel) and Fl-Af1521 (lower panel).
(C) Dose-response and RBN2397 EC_{50} values for recombinant PARP7 and PARP1 ADP-ribosyltransferase activities measured in vitro, using Histone H2A and H2B as a substrate.
(D) Heat maps depicting the effect of RBN2397 (7.6 nM) on the ADP-ribosyltransferase activity of individual PARP family members in vitro (left), and the expression levels of

PARP family members in human prostate cancers (TCGA; RNA-seq data) is also shown (right).
(E) Protein half-life measurements of HA-PARP7 determined in the absence and presence of RBN2397. Cells were pretreated with RBN2397 for 1 hr prior to addition of cycloheximide (0.1 mg/ml). Error bars reflect the standard deviation of biological triplicates.
(F) Auto-ADP-ribosylation of ectopically-expressed PARP7 detected in HA-immunoprecipitates from PC3-AR cells treated with RBN2397. Proteasome inhibition with MG132 (10μM, 4 hrs) was used to increase PARP7 levels.

Fig.2 Growth-inhibitory effect of RBN2397 in AR-positive prostate cancer cells in the presence of androgen.
(A) Cell growth (MTT assay) in response to combinations of RBN2397 and R1881. Each condition reflects eight biological replicates, and the error bars depict the standard deviation. ****, $p<0.0001$; ***, $p<0.001$; n.s., not significant.
(B) RBN2397 dose response growth curves from VCaP, CWR22Rv1, PC3-AR, and PC3 in the presence of the R1881.
(C) Phase contrast microscopy showing the morphology of cells treated with RBN2397 and R1881 (same concentration as in B) for 6 days (slower growing VCaP and CWR22Rv1) and 3 days (faster growing PC3-AR and PC3).
(D) Dead cell detection by Trypan blue staining after culturing cells as in C.

Fig.3 Growth inhibition by RBN2397 is PARP7-dependent and associated with elevated p21 expression.
(A) Treating PC3-AR cells with si*PARP7* partially reduces the growth inhibitory effect of RBN2397. PARP7 knockdown in the cell growth experiments (A-C) was confirmed by immunoblotting using TUBULIN as a loading control (upper panels).
For the cell growth in A-C, each RBN2397 concentration reflects eight biological replicates, error bars show the standard deviation, and the statistical differences between cell lines at each RBN concentration are ****, $p<0.0001$; ***, $p<0.001$; **, <0.01; *, <0.05 (lower panels).
(B, C) Stable knockdown of PARP7 in PC3-AR and CWR22Rv1 cells partially protects from the growth inhibitory effects of RBN2397. CWR22Rv1(*shGFP*) cell growth is copied from Fig. 2B.
(D) Immunoblot detection of CDK inhibitor p21 and PARP7 in prostate cancer lines grown ±R1881 and ±RBN2397 for 24 hrs.
(E) Treating PC3-AR cells with *si-p21* (20 nM) partially reverses the growth inhibitory effect of RBN2397. The expression levels of p21 and PARP7 ±R1881 and ±RBN2397 were determined by immunoblotting (upper panel).
(F) CRISPR knockout of *CDKN1A (p21)* in PC3-AR cells reduces the growth inhibitory effect of RBN2397. The knockout was confirmed by DNA sequencing (not shown) and by immunoblotting for p21 (upper panel).

Fig.4 PARP7 induction using aryl hydrocarbon receptor (AHR) agonists sensitizes prostate cancer cells to growth inhibition by RBN2397.

(A) Effect of RBN2397 on AR- (PC3, DU145) and AR+ (CWR22Rv1, VCaP) prostate cancer lines treated with AHR agonists BBQ and FICZ to induce PARP7. In A and I-J, Each conditions reflects eight biological replicates, error bars show the standard deviation, and ****, $p<0.0001$; ***, $p<0.001$; **, <0.01.
(B) Immunoblotting for PARP7, CYCLIN A, and CYCLIN B after treating cells with AHR agonists and RBN2397.
(C) Phase contrast microscopy showing the morphology of cells treated AHR agonist and RBN2397.
(D-E) Dead cell detection by Trypan blue staining after culturing cells in the presence of AHR agonist and RBN2397.
(F-H) RBN2397 dose response of cell lines grown with BBQ.
(I, J) Stable knockdown of PARP7 blunts the growth inhibitory effects of RBN2397 and BBQ co-treatment in PC3-AR and CWR22Rv1 cells.

Fig.5 The growth inhibitory effect of RBN2397 in prostate cancer cells is not dependent on TBK1 and JAK1/2 kinase function and IFN signaling.
(A) Immunoblot detection of STAT1 and Phospho-STAT1 (left) and cell growth assays (right) in PC3 cells treated as indicated. Ruxolitinib (Ruxo, 0.3 μM) and GSK8612 (GSK, 3 μM) were used to inhibit TBK1 and JAK1/2, respectively, and IFNα (0.3 ng/ml) was used to activate JAK/STAT signaling. PARP7 induction and inhibition was mediated by addition of BBQ and RBN2397.
(B) Phospho-STAT1 levels are not altered detectably by RBN2397 treatment of DU145 cells, and the growth inhibitory effects of RBN2397 are not rescued by blocking TBK1 (GSK) and JAK1/2 (Ruxo) activity. Same treatments and analysis as described for panel A, performed in DU145 cells.
(C) Same treatments and analysis as described for panel A, except R1881 was used to induce PARP7 in PC3-AR cells.

Fig.6 RBN2397 generates a Triton-X100 resistant pool of PARP7.
(A) Biochemical fractionation of PC3-AR cells and immunoblot detection of PARP7, AR, TUBULIN, and LAMIN A after treatment with RBN2397 and R1881.
(B) Biochemical fractionation of PC3 cells and immunoblot detection of PARP7, AHR, TUBULIN, and LAMIN A after treatment with RBN2397 and BBQ.
(C) PARP7 induction with the AHR agonist BBQ sensitizes C4-2b cells to growth inhibition by RBN2397. AHR and endogenous PARP7 were detected by immunoblotting (upper panel), and C4-2b cell growth in response to BBQ and RBN2397 was measured by MTT assay (lower panel).
(D) IP'ed AR from the stable C4-2b(Avi-PARP7) cells with 6 hrs R1881 and RBN2397 treatment is detected by Fl-Af1521. Ectopic, stably expressed Avi-PARP7 is active.
(E) Ectopic, stable expression of Avi-PARP7 in C4-2b cells is sufficient to confer growth sensitivity to RBN2397. Avi-PARP7 expression was detected by immunoblotting (upper panel), and cell growth was measured in the presence of BBQ and RBN2397.

Fig.7 PARP7 expression in prostate cancer.

(A) Violin plots (boxplot inserted) showing *PARP7* expression levels (CPM) in metastatic tumors, primary tumors, and normal prostate. The red line indicates the level of *PARP7*

in the VCaP cell line required for RBN2397-mediated growth inhibition and the gray line shows the basal level of *PARP7* in VCaP cells. P-values calculated for pairwise comparisons using the Wilcoxon test are indicated (***, <0.001; **, <0.01; *, < 0.05; NS, not significant). All compared values come from the recount3 project.

(B) Scatter plots comparing expression of *PARP7* with *AR* and *AHR* in primary tumors (left), metastatic *AR*- tumors (middle), and metastatic *AR*+ tumors (right). Spearman correlation coefficients and p-values are shown on the plots.

(C) Boxplots comparing enrichment scores for HALLMARK_INTERFERON_ALPHA_RESPONSE gene set, calculated using GSVA method between lung (LUAD) and prostate (PRAD) primary tumor samples (left); between high *PARP7* expression (top quartile) and low *PARP7* expression (bottom quartile) in prostate primary tumor samples (middle); between high *PARP7* expression (top quartile) and low *PARP7* expression (bottom quartile) in lung primary tumor samples (right). The p-values from Wilcoxon tests are shown on the plots.

REFERENCES

1. Hottiger, M.O., *Nuclear ADP-Ribosylation and Its Role in Chromatin Plasticity, Cell Differentiation, and Epigenetics.* Annu Rev Biochem, 2015. **84**: p. 227-63.
2. Kraus, W.L., *PARPs and ADP-ribosylation: 60 years on.* Genes Dev, 2020.
3. Luscher, B., et al., *ADP-ribosyltransferases, an update on function and nomenclature.* FEBS J, 2021.
4. Slade, D., *PARP and PARG inhibitors in cancer treatment.* Genes Dev, 2020. **34**(5-6): p. 360-394.
5. Lord, C.J. and A. Ashworth, *PARP inhibitors: Synthetic lethality in the clinic.* Science, 2017. **355**(6330): p. 1152-1158.
6. Rack, J.G.M., L. Palazzo, and I. Ahel, *(ADP-ribosyl)hydrolases: structure, function, and biology.* Genes Dev, 2020. **34**(5-6): p. 263-284.
7. Ahmed, S., et al., *Loss of the Mono-ADP-ribosyltransferase, Tiparp, Increases Sensitivity to Dioxin-induced Steatohepatitis and Lethality.* J Biol Chem, 2015. **290**(27): p. 16824-40.
8. Yang, C.S., et al., *Androgen signaling uses a writer and a reader of ADP-ribosylation to regulate protein complex assembly.* Nat Commun, 2021. **12**(1): p. 2705.
9. Rasmussen, M., et al., *PARP7 and Mono-ADP-Ribosylation Negatively Regulate Estrogen Receptor alpha Signaling in Human Breast Cancer Cells.* Cells, 2021. **10**(3).
10. Bindesboll, C., et al., *TCDD-inducible poly-ADP-ribose polymerase (TIPARP/PARP7) mono-ADP-ribosylates and co-activates liver X receptors.* Biochem J, 2016. **473**(7): p. 899-910.
11. Yamada, T., et al., *Constitutive aryl hydrocarbon receptor signaling*

constrains type I interferon-mediated antiviral innate defense. Nat Immunol, 2016. **17**(6): p. 687-94.
12. Gozgit, J.M., et al., *PARP7 negatively regulates the Type I interferon response in cancer cells and its inhibition triggers antitumor immunity.* Cancer Cell, 2021. **39**(9): p. 1214-1226 e10.
13. Murai, J., et al., *Trapping of PARP1 and PARP2 by Clinical PARP Inhibitors.* Cancer Res, 2012. **72**(21): p. 5588-99.
14. Hopkins, T.A., et al., *PARP1 Trapping by PARP Inhibitors Drives Cytotoxicity in Both Cancer Cells and Healthy Bone Marrow.* Mol Cancer Res, 2019. **17**(2): p. 409-419.
15. Kamata, T., C.S. Yang, and B.M. Paschal, *PARP7 mono-ADP-ribosylates the Agonist Conformation of the Androgen Receptor in the Nucleus.* Biochem J, 2021.
16. Kamata, T., et al., *Detection of ADP-Ribosylation of the Androgen Receptor Using the Recombinant Macrodomain AF1521 from Archaeoglobus fulgidus*, in *Nuclear Receptors: Methods and Experimental Protocols*, M.Z. Badr and M.Z. Badr, Editors. 2019: New York, NY. p. 107-124.
17. Jividen, K., et al., *Genomic analysis of DNA repair genes and androgen signaling in prostate cancer.* BMC Cancer, 2018. **18**(1): p. 960.
18. Lu, S., G. Jenster, and D.E. Epner, *Androgen induction of cyclin-dependent kinase inhibitor p21 gene: role of androgen receptor and transcription factor Sp1 complex.* Mol Endocrinol, 2000. **14**(5): p. 753-60.
19. MacPherson, L., et al., *2,3,7,8-Tetrachlorodibenzo-p-dioxin poly(ADP-ribose) polymerase (TiPARP, ARTD14) is a mono-ADP-ribosyltransferase and repressor of aryl hydrocarbon receptor transactivation.* Nucleic Acids Res, 2013. **41**(3): p. 1604-21.
20. Stockinger, B., et al., *The aryl hydrocarbon receptor: multitasking in the immune system.* Annu Rev Immunol, 2014. **32**: p. 403-32.
21. Kim, T.Y., et al., *Oncogenic potential of a dominant negative mutant of interferon regulatory factor 3.* J Biol Chem, 2003. **278**(17): p. 15272-8.
22. Labrecque, M.P., et al., *Molecular profiling stratifies diverse phenotypes of treatment-refractory metastatic castration-resistant prostate cancer.* J Clin Invest, 2019. **129**(10): p. 4492-4505.
23. Wilks, C., et al., *recount3: summaries and queries for large-scale RNA-seq expression and splicing.* Genome Biol, 2021. **22**(1): p. 323.
24. Hanzelmann, S., R. Castelo, and J. Guinney, *GSVA: gene set variation analysis for microarray and RNA-seq data.* BMC Bioinformatics, 2013. **14**: p. 7.
25. Lu, A.Z., et al., *Enabling drug discovery for the PARP protein family through the detection of mono-ADP-ribosylation.* Biochem Pharmacol, 2019. **167**: p. 97-106.
26. Yang, C.S., et al., *Ligand binding to the androgen receptor induces conformational changes that regulate phosphatase interactions.* Mol Cell Biol, 2007. **27**(9): p. 3390-404.

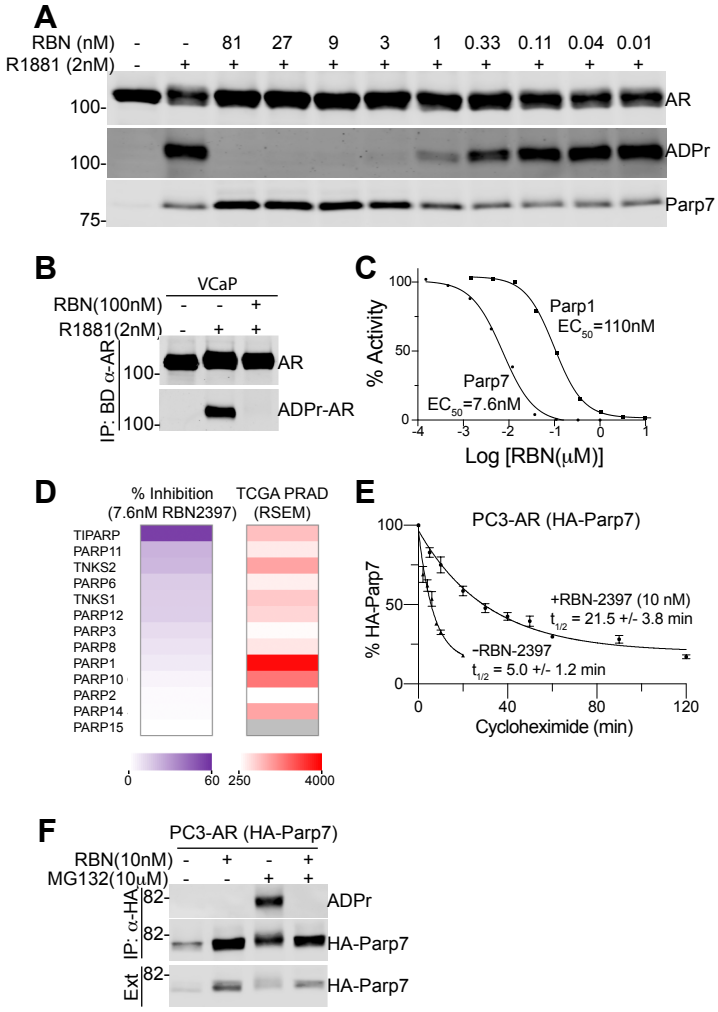
A
RBN (nM) - - 81 27 9 3 1 0.33 0.11 0.04 0.01
R1881 (2nM) - + + + + + + + + + +
100-
100-
75-
AR
ADPr
Parp7
B
VCaP
RBN(100nM) - - +
R1881(2nM) - + +
IP: BD α-AR
100-
100-
AR
ADPr-AR
C
% Activity
Parp1
EC50=110nM
Parp7
EC50=7.6nM
Log [RBN(μM)]
D
% Inhibition
(7.6nM RBN2397)
TCGA PRAD
(RSEM)
TIPARP
PARP11
TNKS2
PARP6
TNKS1
PARP12
PARP3
PARP8
PARP1
PARP10
PARP2
PARP14
PARP15
0
60
250
4000
E
PC3-AR (HA-Parp7)
% HA-Parp7
+RBN-2397 (10 nM)
t1/2 = 21.5 +/- 3.8 min
-RBN-2397
t1/2 = 5.0 +/- 1.2 min
Cycloheximide (min)
F
PC3-AR (HA-Parp7)
RBN(10nM) - + - +
MG132(10μM) - - + +
IP: α-HA
Ext
82-
ADPr
HA-Parp7
HA-Parp7

Figure 1

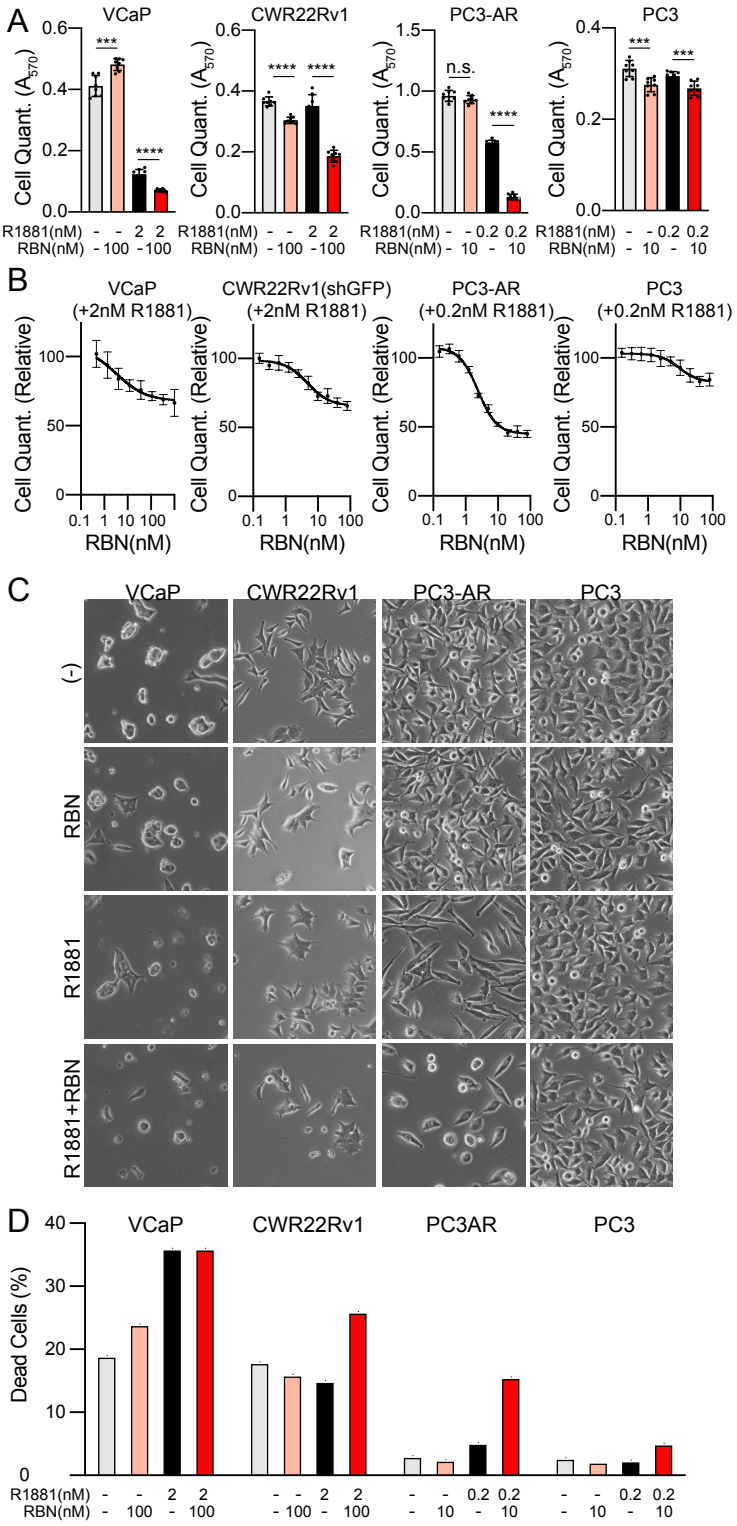
A
VCaP
CWR22Rv1
PC3-AR
PC3
Cell Quant. (A_{570})
***
****
n.s.
R1881(nM) - - 2 2
RBN(nM) - 100 - 100
R1881(nM) - - 0.2 0.2
RBN(nM) - 10 - 10
B
VCaP (+2nM R1881)
CWR22Rv1(shGFP) (+2nM R1881)
PC3-AR (+0.2nM R1881)
PC3 (+0.2nM R1881)
Cell Quant. (Relative)
RBN(nM)
C
VCaP
CWR22Rv1
PC3-AR
PC3
(-)
RBN
R1881
R1881+RBN
D
VCaP
CWR22Rv1
PC3AR
PC3
Dead Cells (%)
R1881(nM) - - 2 2
RBN(nM) - 100 - 100
R1881(nM) - - 0.2 0.2
RBN(nM) - 10 - 10

Fig 2

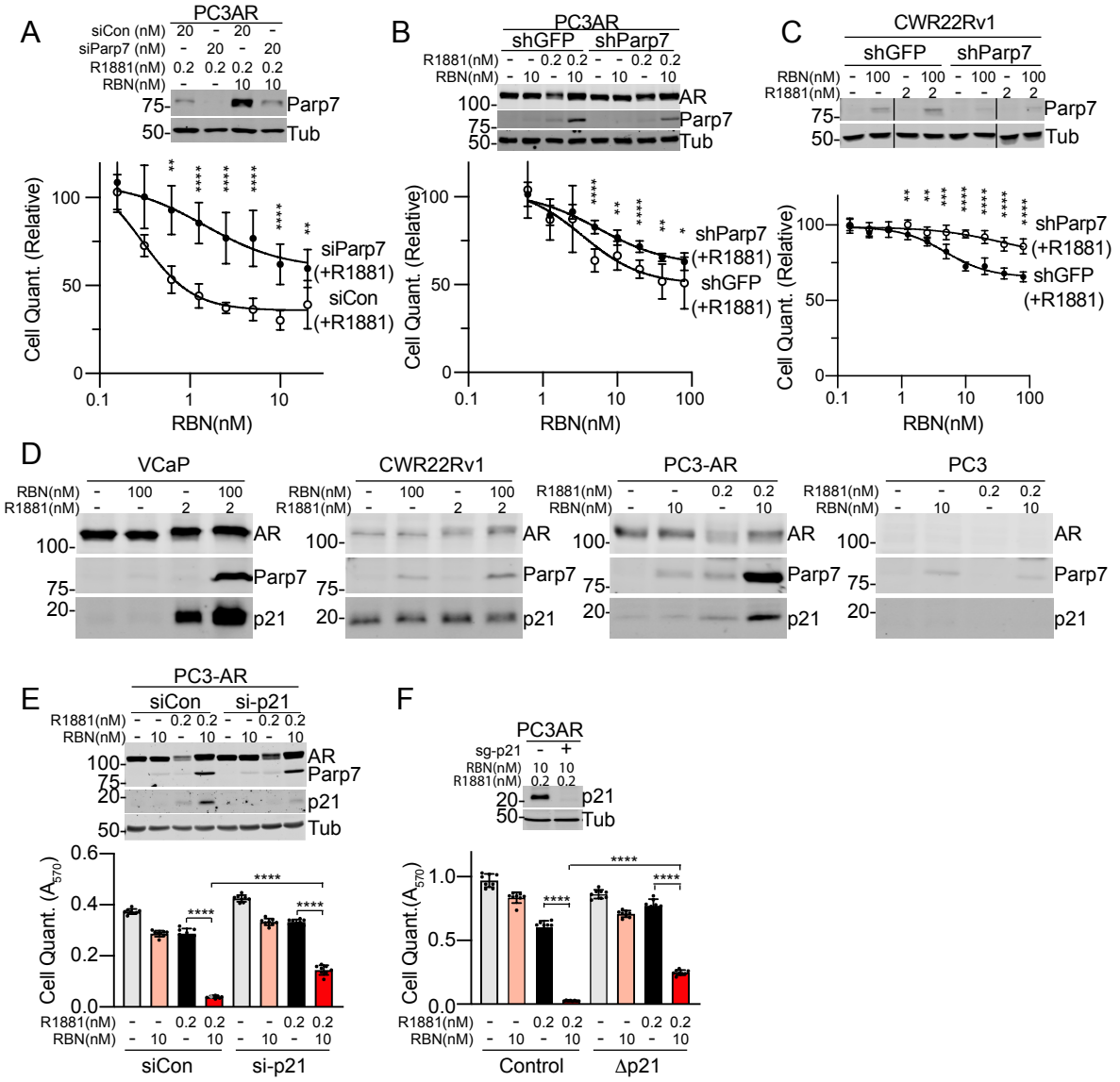
A
PC3AR
siCon (nM) 20 - 20 -
siParp7 (nM) - 20 - 20
R1881(nM) 0.2 0.2 0.2 0.2
RBN(nM) - - 10 10
75-
50-
Parp7
Tub
Cell Quant. (Relative)
RBN(nM)
siParp7 (+R1881)
siCon (+R1881)
B
PC3AR
shGFP shParp7
R1881(nM) - - 0.2 0.2 - - 0.2 0.2
RBN(nM) - 10 - 10 - 10 - 10
100-
75-
50-
AR
Parp7
Tub
shParp7 (+R1881)
shGFP (+R1881)
C
CWR22Rv1
shGFP shParp7
RBN(nM) - 100 - 100 - 100 - 100
R1881(nM) - - 2 2 - - 2 2
Parp7
Tub
shParp7 (+R1881)
shGFP (+R1881)
D
VCaP
CWR22Rv1
PC3-AR
PC3
RBN(nM)
R1881(nM)
AR
Parp7
p21
E
PC3-AR
siCon si-p21
R1881(nM) - - 0.2 0.2 - - 0.2 0.2
RBN(nM) - 10 - 10 - 10 - 10
AR
Parp7
p21
Tub
Cell Quant. (A_{570})
siCon
si-p21
F
PC3AR
sg-p21 - +
RBN(nM) 10 10
R1881(nM) 0.2 0.2
p21
Tub
Control
Δp21

Fig 3

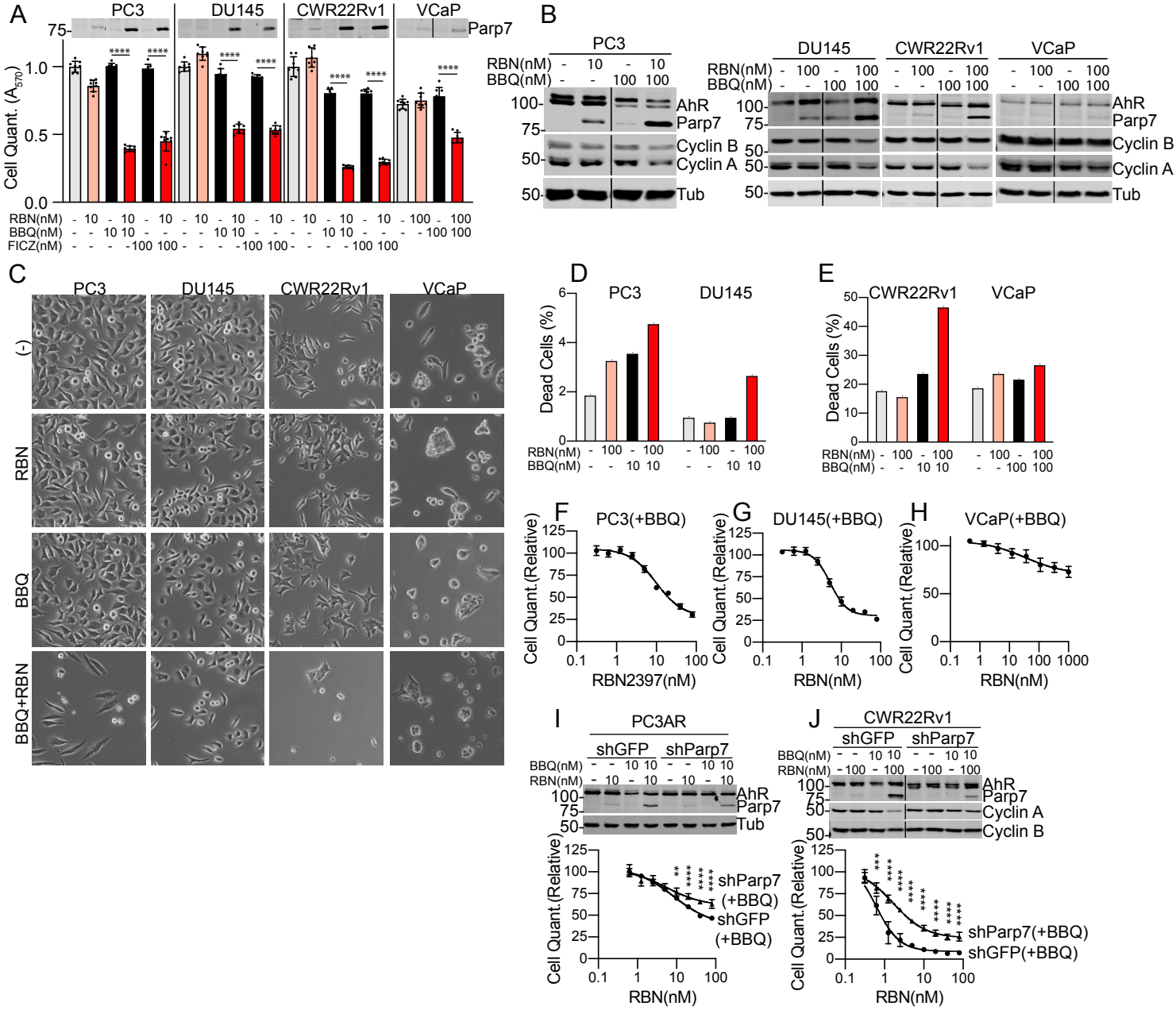
A
PC3
DU145
CWR22Rv1
VCaP
Parp7
Cell Quant. (A_{570})
RBN(nM)
BBQ(nM)
FICZ(nM)
B
PC3
DU145
CWR22Rv1
VCaP
RBN(nM)
BBQ(nM)
AhR
Parp7
Cyclin B
Cyclin A
Tub
C
PC3
DU145
CWR22Rv1
VCaP
(-)
RBN
BBQ
BBQ+RBN
D
PC3
DU145
Dead Cells (%)
E
CWR22Rv1
VCaP
Dead Cells (%)
F
PC3(+BBQ)
Cell Quant.(Relative)
RBN2397(nM)
G
DU145(+BBQ)
Cell Quant.(Relative)
RBN(nM)
H
VCaP(+BBQ)
Cell Quant.(Relative)
RBN(nM)
I
PC3AR
shGFP
shParp7
BBQ(nM)
RBN(nM)
AhR
Parp7
Tub
Cell Quant.(Relative)
shParp7 (+BBQ)
shGFP (+BBQ)
RBN(nM)
J
CWR22Rv1
shGFP
shParp7
BBQ(nM)
RBN(nM)
AhR
Parp7
Cyclin A
Cyclin B
Cell Quant.(Relative)
shParp7(+BBQ)
shGFP(+BBQ)
RBN(nM)

Fig 4

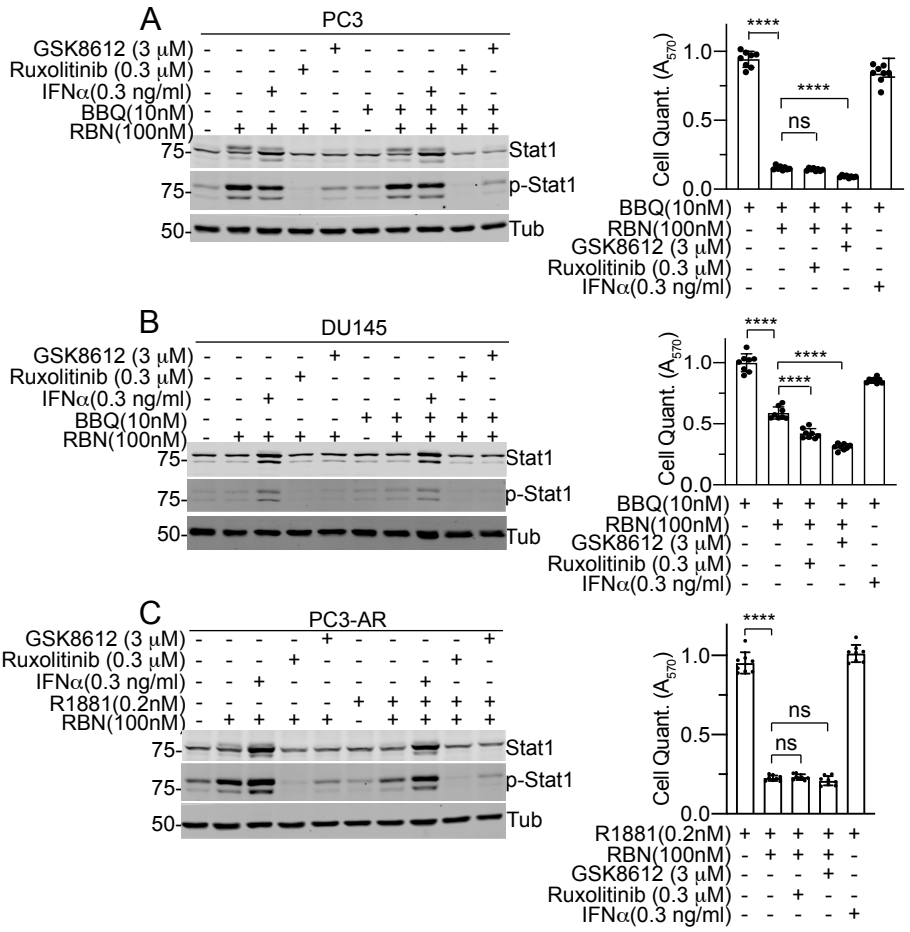
A
PC3
GSK8612 (3 μM)
Ruxolitinib (0.3 μM)
IFNα(0.3 ng/ml)
BBQ(10nM)
RBN(100nM)
75-
75-
50-
Stat1
p-Stat1
Tub
Cell Quant. (A_{570})
1.0
0.5
0.0
****
****
ns
B
DU145
****
****
****
C
PC3-AR
R1881(0.2nM)
ns
ns

Fig 5

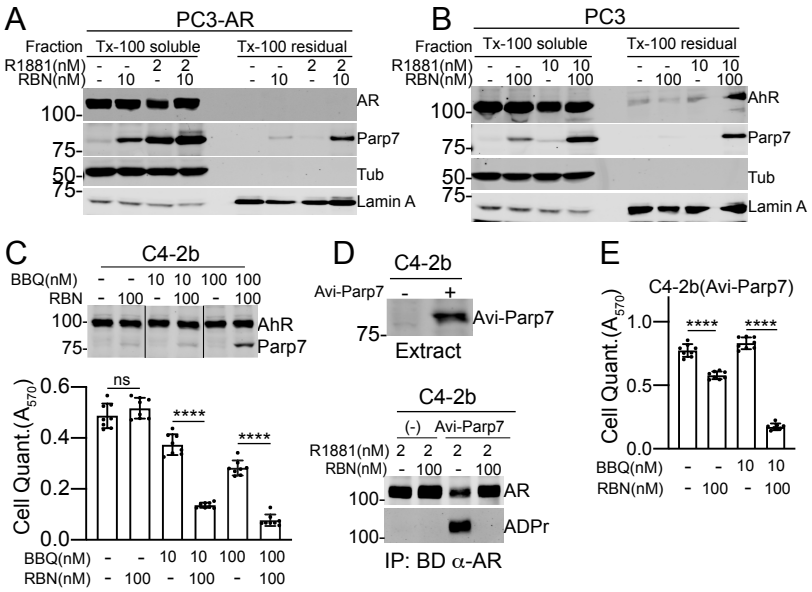
A
PC3-AR
Fraction
Tx-100 soluble
Tx-100 residual
R1881(nM)
RBN(nM)
AR
Parp7
Tub
Lamin A
B
PC3
C
C4-2b
BBQ(nM)
RBN
AhR
Parp7
Cell Quant.(A570)
ns
****
D
C4-2b
Avi-Parp7
Extract
(-)
R1881(nM)
RBN(nM)
ADPr
IP: BD α-AR
E
C4-2b(Avi-Parp7)

Fig 6

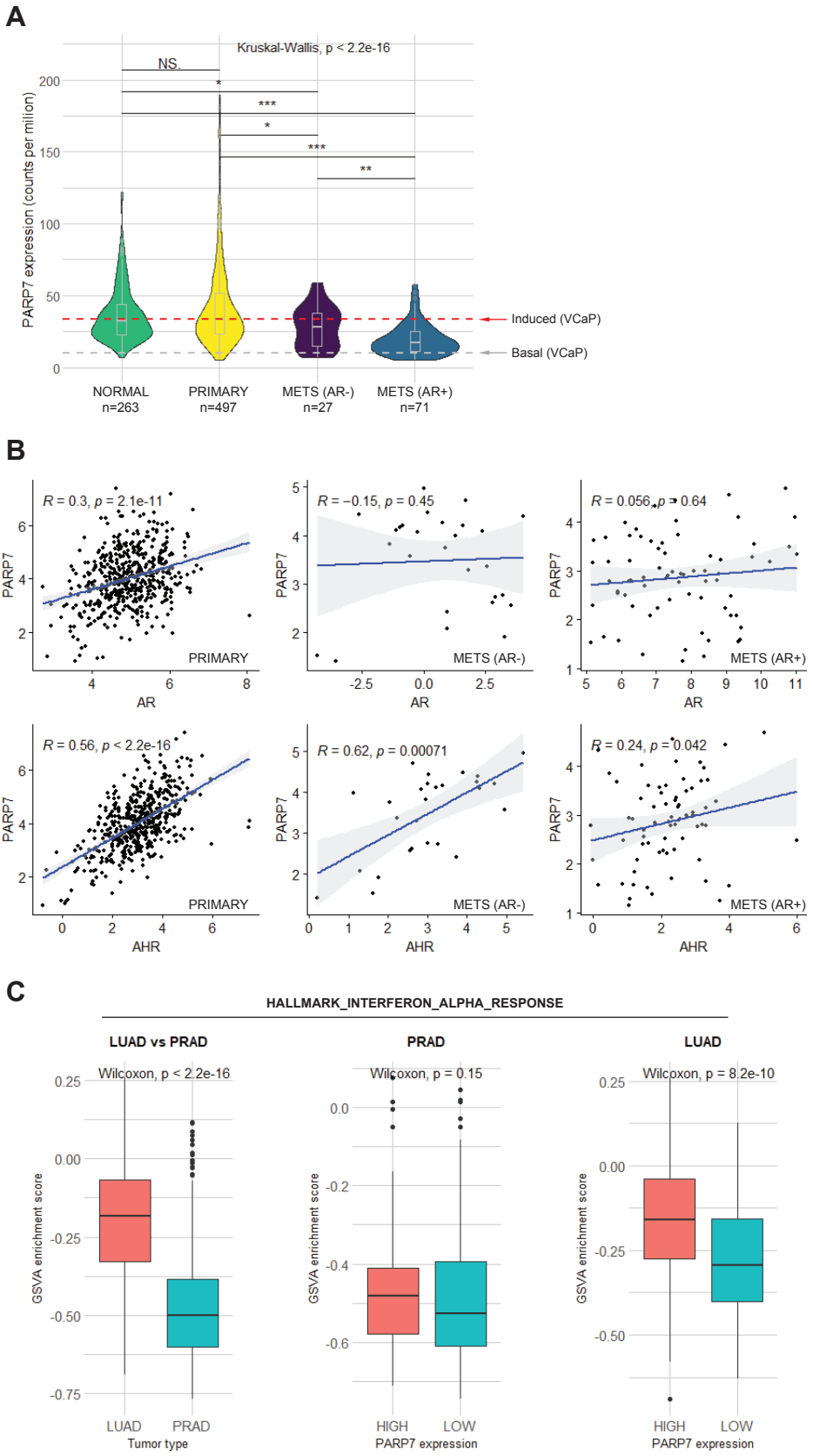
A
Kruskal-Wallis, p < 2.2e-16
NS.
PARP7 expression (counts per milion)
Induced (VCaP)
Basal (VCaP)
NORMAL n=263
PRIMARY n=497
METS (AR-) n=27
METS (AR+) n=71
B
R = 0.3, p = 2.1e-11
PRIMARY
R = −0.15, p = 0.45
METS (AR-)
R = 0.056, p = 0.64
METS (AR+)
R = 0.56, p < 2.2e-16
R = 0.62, p = 0.00071
R = 0.24, p = 0.042
PARP7
AR
AHR
C
HALLMARK_INTERFERON_ALPHA_RESPONSE
LUAD vs PRAD
Wilcoxon, p < 2.2e-16
PRAD
Wilcoxon, p = 0.15
LUAD
Wilcoxon, p = 8.2e-10
GSVA enrichment score
LUAD
PRAD
Tumor type
HIGH
LOW
PARP7 expression

Fig 7